Measurement of interferences associated with the detection of the hydroperoxy radical in the atmosphere using laser-induced fluorescence

Michelle M. Lew[1], Sebastien Dusanter[2,3], and Philip S. Stevens[1,3]

(1) Department of Chemistry, Indiana University, Bloomington, IN, USA

(2) IMT Lille Douai, Univ. Lille, SAGE - Département Sciences de l'Atmosphère et Génie de l'Environnement, 59000 Lille, France

(3) School of Public and Environmental Affairs, Indiana University, Bloomington, IN, USA

Correspondence to: Philip S. Stevens (pstevens@indiana.edu)

1 **Abstract.** One technique used to measure concentrations of the hydroperoxy radical (HO_2) in the atmosphere

2 involves chemically converting it to OH by addition of NO and subsequent detection of OH. However, some

3 organic peroxy radicals (RO_2) can also be rapidly converted to HO_2 (and subsequently OH) in the presence of

4 NO, interfering with measurements of ambient HO_2 radical concentrations. This interference must be

5 characterized for each instrument to determine to what extent various RO_2 radicals interfere with measurements

6 of HO_2 and to assess the impact of this interference on past measurements. The efficiency of RO_2 to HO_2

7 conversion for the Indiana University Laser-Induced Fluorescence – Fluorescence Assay by Gas Expansion (IU-

8 FAGE) instrument was measured for a variety of RO_2 radicals. Known quantities of OH and HO_2 radicals were

9 produced from the photolysis of water vapor at 184.9 nm, and RO_2 radicals were produced by the reaction of

10 several volatile organic compounds with OH. The conversion efficiency of RO_2 radicals to HO_2 was measured

11 when NO was added to the sampling cell for conditions employed during several previous field campaigns. For

12 these conditions, approximately 80% of alkene derived RO_2 radicals and 20% of alkane derived RO_2 radicals were

13 converted to HO_2. Based on these measurements, interferences from various RO_2 radicals contributed to

14 approximately 35% of the measured HO_2 signal during the Mexico City Metropolitan Area (MCMA) 2006

15 campaign, where the measured VOCs consisted of a mixture of saturated and unsaturated species. However, this

16 interference can contribute more significantly to the measured HO_2 signal in forested environments dominated by

17 unsaturated biogenic emissions such as isoprene.

1 Introduction

The hydroxyl radical (OH) is one of the primary oxidants in the atmosphere (Levy, 1972). The reaction of OH radicals with volatile organic compounds (VOCs) leads to the production of peroxy radicals, both the hydroperoxy radical (HO_2) and organic peroxy radicals (RO_2), which in the presence of nitrogen oxides ($NO_x = NO + NO_2$) can lead to the production of ozone and secondary organic aerosols in the atmosphere. As a consequence, the development of effective control strategies for the formation of these pollutants requires an accurate understanding of the OH, HO_2, and RO_2 radical chemistry in the atmosphere. Measurements of OH and HO_2 (together HO_x) can provide a robust test of our understanding of this complex oxidation chemistry.

Multiple field campaigns have been conducted over the years measuring OH and HO_2 radicals in both urban and forested environments. While much attention has been focused on discrepancies between measured and modeled OH concentrations (Rohrer et al., 2014), the agreement between measured and modeled HO_2 concentrations has been highly variable. In urban environments, measured HO_2 concentrations were sometimes found to agree with model predictions (Shirley et al., 2006; Emmerson et al., 2007; Dusanter et al., 2009b; Michoud et al., 2012; Lu et al., 2013; Ren et al., 2013; Griffith et al., 2016), while other times the measurements were found to be both lower (George et al., 1999; Konrad et al., 2003) and higher than model predictions (Martinez et al., 2003; Ren et al., 2003; Emmerson et al., 2005; Kanaya et al., 2007a; Chen et al., 2010; Sheehy et al., 2010; Czader et al., 2013; Griffith et al., 2016). In forested environments, measured HO_2 concentrations were sometimes found to agree with model predictions (Tan et al., 2001; Ren et al., 2005; 2006), but were often found to be either lower (Carslaw et al., 2001; Kanaya et al., 2007b; Whalley et al., 2011; Kanaya et al., 2012; Mao et al., 2012; Griffith et al., 2013), or higher than model predictions (Carslaw et al., 2001; Kubistin et al., 2010; Kim et al., 2013; Hens et al., 2014).

These results question our understanding of HO_x radical chemistry and the ability of models to simulate future changes in the chemical composition of the atmosphere. However, a recent intercomparison of several instruments measuring HO_2 found that the agreement between the different instruments was variable, although the measurements were highly correlated (Fuchs et al., 2010). While the differences were within the combined uncertainties of the measurements, there were several measurement periods when the differences could not be explained by instrumental uncertainties. These results suggested the possibility of potential interferences in the HO_2 measurement technique.

Laser-induced fluorescence using the Fluorescence Assay by Gas Expansion technique (LIF-FAGE) is a common method for measuring HO_2 radicals in the atmosphere. In this technique HO_2 radicals are measured

indirectly after sampling ambient air at low pressure through chemical conversion to OH by addition of NO as shown in reaction R1 and subsequent detection of OH by LIF:

$$HO_2 + NO \rightarrow OH + NO_2 \tag{R1}$$

It was previously believed that the detection of HO_2 radicals using the LIF-FAGE technique was free from interferences from the reaction of RO_2 radicals with NO, as model simulations and measurements suggested that the rate of conversion of RO_2 radicals to HO_2 by reactions R2 and R3 and subsequent conversion to OH through reaction R1 was negligible due to the slow rate of reaction R3 under the reduced oxygen concentration in the low pressure LIF-FAGE cell and the short reaction time between injection of NO and detection of OH (Heard and Pilling, 2003).

$$RO_2 + NO \rightarrow RO + NO_2 \tag{R2}$$

$$RO + O_2 \rightarrow R'O + HO_2 \tag{R3}$$
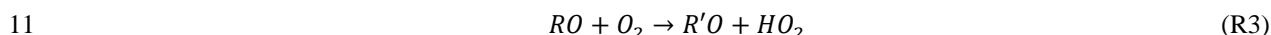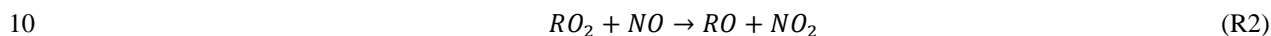
For example, RO_2 radicals produced from the OH-initiated oxidation of small alkanes were found to produce a negligible yield of HO_2 (Stevens et al., 1994; Kanaya et al., 2001; Tan et al., 2001; Creasey et al., 2002; Holland et al., 2003).

However, recent laboratory studies have shown that there are interferences associated with measurements of HO_2 using this technique from the conversion of RO_2 radicals derived from the OH-initiated oxidation of alkenes and aromatics to HO_2 (and subsequently OH) by reaction with NO. Measured RO_2 to HO_2 conversion efficiencies of 95% for the peroxy radicals derived from the OH-initiated oxidation of propene and 86% for the peroxy radicals derived from the OH-initiated oxidation of benzene have been reported (Fuchs et al., 2011). The high conversion efficiency of alkene-based peroxy radicals to HO_2 is due to the ability of the β-hydroxyalkoxy radicals produced from reaction R2 to rapidly decompose forming a hydroxyalkyl radical which then reacts rapidly with O_2 leading to the production of a carbonyl compound and HO_2 (Fuchs et al., 2011; Whalley et al., 2013). The conversion efficiency depends on the instrumental characteristics and the configurations employed (Fuchs et al., 2011; Whalley et al., 2013). As a result, this interference must be characterized for all LIF-FAGE instruments for the accurate analysis of ambient HO_2.

This paper will describe the characterization of the RO_2 interferences associated with the Indiana University LIF-FAGE instrument under several past campaign configurations. These include the Mexico City Metropolitan Area (MCMA) campaign in 2006 (Dusanter et al., 2009a; 2009b), the Community Atmosphere-Biosphere INteractions EXperiment (CABINEX) in 2009 (Griffith et al., 2013), and the California Research at the Nexus of Air Quality and Climate Change campaign in Los Angeles (CalNex-LA) in 2010 (Griffith et al.,

1 2016). The impact of this interference on the previously published results from the MCMA-2006 campaign and a

2 reanalysis of these HO_2 measurements will be discussed.

3 **2 Experimental Section**

4 **2.1 Instrument description**

5 The Indiana University LIF-FAGE instrument (IU-FAGE) has been described in detail previously (Dusanter et

6 al., 2008; 2009a; Griffith et al., 2013; 2016). In the LIF-FAGE technique, OH radicals are detected by laser-

7 induced fluorescence after expansion of ambient air to low pressure. This enhances the OH fluorescence lifetime,

8 allowing temporal filtering of the fluorescence from laser scatter (Heard and Pilling, 2003). A diagram of the IU-

9 FAGE detection cell is illustrated in Fig. 1. Ambient air is expanded through an orifice between 0.635 mm and

10 1.016 mm diameter located at the top of a cylindrical nozzle (5 cm in diameter and 20 cm long). The size of the

11 orifice was kept unchanged during each campaign but was varied between the different campaigns reported here.

12 Two scroll pumps (Edwards XDS 35i) connected in parallel maintain a pressure inside the cell between 4 and 7.5

13 Torr depending on the sampling size of the orifice and the pumping speed, resulting in a flow rate between 3 and

14 10 SLPM through the sampling nozzle.

15 The original IU-FAGE laser system used in this study and in the MCMA-2006 campaign consisted of a

16 Spectra Physics Navigator II YHP40-532Q diode-pumped Nd:YAG laser that produced approximately 5.5W of

17 radiation at 532 nm at a repetition rate of 5 kHz. This laser pumped a Lambda Physik Scanmate 1 dye laser

18 (Rhodamine 640, 0.25 g L^{-1} in isopropanol) that produced tunable radiation around 616 nm, which was frequency

19 doubled to generate 2 to 20 mW of radiation at 308 nm (~20 ns pulse width). This laser system was recently

20 replaced with a Spectra Physics Navigator II YHP40-532Q that produces approximately 8 W of radiation at 532

21 nm at a repetition rate of 10 kHz that pumps a Sirah Credo Dye laser (255 mg/L of Rhodamine 610 and 80 mg/L

22 of Rhodamine 101 in ethanol), resulting in 40 to 100 mW of radiation at 308 nm. Measurements of the conversion

23 efficiencies were similar for the two laser systems. After exiting the dye laser, the beam was focused onto the

24 entrance of a 12 m optical fiber to transmit the radiation to the sampling cell. In the detection cell, the laser crosses

25 the expanded air perpendicular to the flow in a White cell configuration with approximately 24 passes.

26 OH radicals are excited using the $A^2\Sigma^+$ υ'=0 ← $X^2\Pi$ υ"= 0 transition near 308 nm (Stevens et al., 1994).

27 The net signal is measured by turning the wavelength on- and off-resonance in successive modulation cycles. A

28 reference cell where OH is produced by thermal dissociation of water vapor is used to ensure that the laser is tuned

29 on and off the OH transition. The OH fluorescence is detected using a microchannel plate photomultiplier tube

1 (MCP-PMT) detector (Hamamatsu R5946U-50), a preamplifier (Stanford Research System SR445) and a gated

2 photon counter (Stanford Research Systems SR 400). The MCP-PMT is switched off during the laser pulse

3 through the use of electronic gating allowing the OH fluorescence to be temporally filtered from laser scattered

4 light.

5   A Teflon injector located approximately 2.5 cm below the inlet and 17.5 cm above the detection axis

6 (Fig. 1) allowed for the addition of NO (Matheson, 99.8%) to convert ambient HO_2 to OH through reaction R1.

7 The fraction of HO_2 (C_{HO2}) converted into OH was measured during calibration experiments (Dusanter et al.,

8 2008). The NO flow (approximately $1-3\times10^{13}$ cm^{-3}) maximized the conversion of HO_2 into OH while minimizing

9 the removal of OH by the OH + NO reaction.

10 **2.2 Instrument Calibration for OH and HO$_2$**

11 The IU-FAGE instrument is calibrated by producing known quantities of OH and HO_2 radicals from the photolysis

12 of water vapor in air (reactions R4 and R5) (Dusanter et al., 2008):

$$H_2O + hv \text{ (184.9 nm)} \rightarrow H + OH \tag{R4}$$

$$H + O_2 \rightarrow HO_2 \tag{R5}$$
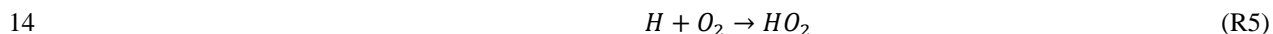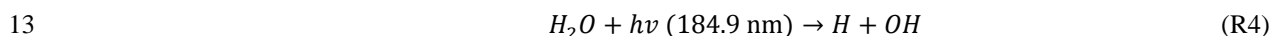
15 The calibration source consists of an aluminum flow reactor ($1.27\times1.27\times30$ cm) equipped with quartz windows

16 on two sides (Fig. 2). The light source consists of a low-pressure mercury lamp (UVP Inc.) housed in an aluminum

17 cartridge that is continuously purged with dry nitrogen to prevent light absorption by gases in addition to helping

18 to stabilize the lamp temperature. The radiation from the lamp passes through a bandpass filter centered at 185

19 nm (Acton Research) prior to entering the reactor and is detected by a photodiode. The lamp housing can be

20 adjusted along the length of the calibrator to measure the loss of radicals between the source region and the exit

21 of the calibrator.

22   The concentration of OH and HO_2 radicals produced by the calibration source can be determined from

23 the following equation:

$$[OH] = [HO_2] = [H_2O] \cdot \sigma_{H_2O} \cdot \varphi_{OH+H} \cdot F \cdot t \tag{1}$$

25 In this equation φ_{OH+H} is the quantum yield of OH from water photolysis, and σ_{H2O} is the absorption cross section

26 of water (7.14×10^{-20} cm^{-2} molecule^{-1} (Cantrell et al., 1997; Hofzumahaus et al., 1997; Creasey et al., 2000)). The

27 product of the photon flux (F) and the photolysis time (t) can be determined from oxygen actinometry, as the

28 photolysis of oxygen at 185 nm leads to the production of ozone (reactions R6 and R7) (Okabe, 1978):

$$O_2 + h\nu\ (184.9\ \text{nm}) \rightarrow 2O(^3P) \tag{R6}$$

$$O_2 + O(^3P) + M \rightarrow O_3 + M \tag{R7}$$
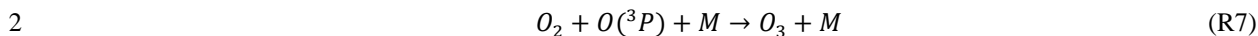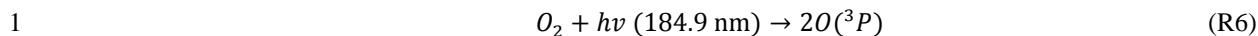
The concentration of HO_x radicals can thus be calculated from measured concentrations of water and ozone using Eq. (2) (Heard and Pilling, 2003; Holland et al., 2003):

$$[OH] = [HO_2] = [H_2O] \cdot \sigma_{H_2O} \cdot \varphi_{OH+H} \cdot \frac{[O_3]}{\varphi_{O_3} \cdot \sigma_{O_2} \cdot [O_2]} \tag{2}$$

Here φ_{O3} is the quantum yield of O_3 from oxygen photolysis and and σ_{O2} is the absorption cross sections of O_2, which must be experimentally determined for each penlamp due to the overlap of the highly structured absorption spectrum of O_2 and the lineshape of the emission at 184.9 nm. The lineshape depends on the operating conditions of the lamp as a result of line reversal and potential fluorescence of the fused silica envelope (Cantrell et al., 1997; Hofzumahaus et al., 1997; Lanzendorf et al., 1997).

2.3 Measurement of the RO$_2$ conversion efficiency to HO$_2$

Various alkenes (isoprene, methyl vinyl ketone, methacrolein, methyl ethyl ketone, ethene, trans-2-butene, tetramethylethylene), alkanes (propane, butane, octane), and aromatic compounds (toluene) were used to measure the conversion efficiency of RO_2 radicals to HO_2. These VOCs were added to the main calibrator flow, either by direct addition of a gas mixture or by bubbling air through the liquid compound (Tables S1 and S2), approximately 190 ms prior to the radical source to ensure that the added VOC was well mixed into the humid air flow before photolysis within the calibration source. The concentration of each VOC added to the calibrator was increased to react and remove the majority of the OH produced in the calibrator, resulting in RO_2 concentrations that were approximately equal to the concentration of OH reacted away. These RO_2 radicals are then sampled into the IU-FAGE instrument. Addition of NO inside the detection axis converts a fraction of the RO_2 radicals to HO_2 through reactions R2 and R3. Since RO_2 is produced together with HO_2 in the calibrator, there is a subsequent conversion of both RO_2 and HO_2 into OH in the IU-FAGE cell, which is then detected by LIF.

Figure 3 illustrates two typical experiments designed to measure the conversion efficiency of RO_2 radicals to HO_2 in the IU-FAGE instrument. The total HO_x signal is defined as the sum of the total OH (S_{OH}) and HO_2 (S_{HO2}) produced by the mercury penlamp in the absence of the added VOC (Eq. (3)):

$$S_{HO_x} = S_{HO_2} + S_{OH} \tag{3}$$

1 The OH concentration produced by the penlamp is measured at the beginning, middle, and at the end of each

2 experiment to ensure that the concentrations remained stable (experimental mode 1 in Fig. 3). Once the OH signal

3 (S_{OH}) stabilizes, NO is added internally to the detection cell to convert HO_2 into OH and measure the total HO_x

4 signal (S_{HOx}) (mode 2 in Fig. 3). The conversion efficiency of HO_2 to OH is defined by Eq. (4):

$$C_{HO_2 \rightarrow OH} = \frac{S_{HO_x} - S_{OH}}{S_{OH_0}} = \frac{S_{HO_2}}{S_{OH_0}} \qquad (4)$$

6 S_{OH0} is the OH signal after accounting for the loss of OH on the walls of the calibrator (approximately 20%). The

7 wall loss for HO_2 is negligible in the calibrator (Dusanter et al., 2008).

8   Next, internal NO addition is stopped and the OH signal is measured again to ensure the stability of

9 radical production during the experiment. The VOC is then added to the calibration system resulting in a decrease

10 in the observed OH signal (mode 3 in Fig. 3). The remaining OH signal in the presence of the VOC is denoted as

11 $S_{OH+VOC.}$ For alkenes such as isoprene, the fast reaction with OH results in an almost total removal of OH radicals

12 from the calibration source and S_{OH+VOC} is close to zero. However, for less reactive alkanes such as butane, the

13 added VOC concentration was often not sufficient to completely remove OH radicals due to the short reaction

14 time in the calibrator, resulting in a non-zero S_{OH+VOC} signal. The conversion efficiency in which OH radicals are

15 converted to RO_2 radicals ($C_{OH \rightarrow RO2}$) is defined by Eq. (5), derived from integrating the expressions for the rate of

16 OH loss and the rate of RO_2 production from the OH +VOC reaction:

$$C_{OH \rightarrow RO_2} = \frac{[RO_2]}{[OH]_0} = \frac{F_{OH} - k_w t}{F_{OH}} (1 - e^{-F_{OH}}) \qquad F_{OH} = ln\left(\frac{S_{OH_0}}{S_{OH+VOC}}\right) \qquad (5)$$

18 Here $k_w t$ is the product of the rate constant for reaction of OH radicals on the wall of the calibration source with

19 the reaction time t, reflecting the measured loss of OH on the walls of the calibrator (Dusanter et al., 2008).

20   The subsequent addition of NO to the detection cell will convert a fraction of RO_2 radicals and HO_2

21 radicals to OH (mode 4 in Fig. 3). The conversion efficiency of RO_2 to OH ($C_{RO2 \rightarrow OH}$) is determined by

22 multiplying the fraction of RO_2 radicals converted to HO_2 ($f_{RO2 \rightarrow HO2}$) with the conversion efficiency of HO_2 to

23 OH ($C_{HO2 \rightarrow OH}$):

$$C_{RO_2 \rightarrow OH} = f_{RO_2 \rightarrow HO_2} \cdot C_{HO_2 \rightarrow OH} \qquad (6)$$

25 The signal due to RO_2 radicals (S_{RO2}) is defined as the original OH signal (S_{OHo}) multiplied by the conversion

26 efficiency of OH radicals to RO_2 radicals ($C_{OH \rightarrow RO2}$) and multiplied by the conversion efficiency of RO_2 to OH

27 ($C_{RO2 \rightarrow OH}$) (Eq. (7)):

$$S_{RO_2} = S_{OH_0} \cdot C_{OH \to RO_2} \cdot C_{RO_2 \to OH} \tag{7}$$

For OH +VOC reactions that lead to the production of HO_2 with a yield of y (OH + benzene and toluene for example (Klotz et al., 1998; Nehr et al., 2011)), the OH to RO_2 conversion efficiency (C_{OH+VOC}) must be multiplied by the overall yield $(1-y)$ of RO_2 radicals produced from the OH +VOC reaction. Taking this yield into account, the signals due to RO_2 and HO_2 radicals become:

$$S_{RO_2} = S_{OH_0} \cdot C_{OH \to RO_2} \cdot (1 - y) \cdot C_{RO_2 \to OH} \tag{7a}$$

$$S_{HO_2\ total} = S_{OH_0} \cdot C_{OH \to RO_2} \cdot y \cdot C_{HO_2 \to OH} + S_{HO_2} \tag{8}$$

The measured OH signal under these conditions (S_{ROx}) reflects the contribution of RO_2, HO_2, and unreacted OH radicals (experimental mode 4):

$$S_{RO_x} = S_{RO_2} + S_{HO_2\ total} + S_{OH+VOC} \tag{9}$$

$$S_{RO_x} = \left(S_{OH_0} \cdot C_{OH \to RO_2} \cdot (1 - y) \cdot C_{RO_2 \to OH} \right) + \left(S_{OH_0} \cdot C_{OH \to RO_2} \cdot y \cdot C_{HO_2 \to OH} + S_{HO_2} \right) + S_{OH+VOC} \tag{9a}$$

Combining equations 3, 6, and 9a results in an expression for the fraction of RO_2 radicals converted to HO_2 ($f_{RO2 \to HO2}$) that can be expressed as the measured signals for each experimental mode (S_{OH}, S_{HOx}, S_{OH+VOC}, S_{ROx}) as seen in Eq. (10):

$$f_{RO_2 \to HO_2} = \frac{S_{RO_x} - S_{HO_x} + S_{OH} - S_{OH+VOC} - S_{OH_0} \cdot C_{OH \to RO_2} \cdot y \cdot C_{HO_2 \to OH}}{S_{OH_0} \cdot C_{OH \to RO_2} \cdot (1 - y) \cdot C_{HO_2 \to OH}} \tag{10}$$

When the yield of HO_2 from the OH + VOC reaction is zero ($y = 0$), and under conditions where all the OH radicals are converted to RO_2 ($S_{OH+VOC} = 0$), the above equation (with Eq. 3 and 4) simplifies to the following:

$$f_{RO_2 \to HO_2} = \frac{S_{RO_x} - S_{HO_x} + S_{OH}}{S_{OH_0} \cdot C_{OH \to RO_2} \cdot C_{HO_2 \to OH}} = \frac{S_{RO_x} - S_{HO_x} + S_{OH}}{(S_{HO_x} - S_{OH}) \cdot C_{OH \to RO_2}} \tag{11}$$

Because this method cannot distinguish between the different peroxy radicals that could be produced from each OH + VOC reaction, the measured conversion efficiency reflects the average conversion efficiency of all peroxy radicals for a given VOC.

1 **3 Results**

2 The pressure and flow conditions for the three campaigns conducted with the IU LIF-FAGE instrument are

3 summarized in Table 1. For each characterization, the flow rate of NO addition was kept constant at 1 sccm in

4 order to determine the impact of the different operating conditions on the measured RO_2-to-HO_2 conversion

5 efficiencies. This is the NO flow rate used during the MCMA-2006, CABINEX and CalNex campaigns, and

6 resulted in HO_2-to-OH conversion efficiencies that were similar to that measured during both the CABINEX and

7 the CalNex campaigns. However, the measured HO_2-to-OH conversion efficiency for the MCMA-2006 campaign

8 configuration in these experiments was approximately 20% lower than that previously reported (Dusanter et al.,

9 2008; 2009a). The reason for this discrepancy is unclear, and may indicate problems in precisely recreating the

10 flow conditions during this campaign in these laboratory experiments. In addition, the NO flow rate was varied

11 during MCMA-2006 in order to maximize the HO_2-to-OH conversion efficiency and to quantify the photolytic

12 interference associated with high NO concentrations in the detection cell. Thus it is possible that the actual flow

13 rate used to maximize the conversion efficiency was slightly greater than the 1 sccm reported. Since it is not

14 known whether the flow was greater than the 1 sccm that was measured, or whether the flow conditions led to

15 more efficient mixing, we chose to conduct the experiments using the measured 1 sccm flow rate. It is difficult to

16 quantify how the higher HO_2-to-OH conversion efficiency measured during MCMA-2006 would translate into

17 the various RO_2-to-HO_2 conversion efficiencies, although it is likely that many of them would be larger. As a

18 result, the conversion efficiencies measured in this study for the MCMA-2006 configuration may represent a

19 lower limit to the actual conversion efficiencies during the campaign.

20 The RO_2 conversion efficiency into HO_2 ($f_{RO2 \rightarrow HO2}$) measured for the inlet conditions for the MCMA

21 2006, CABINEX, and CalNex campaigns are summarized in Table 2 and represent the results of several

22 experiments similar to those illustrated in Fig. 3, with the uncertainty representing one standard error of the mean

23 of the measurements. The largest RO_2 interference was observed for the CalNex inlet conditions where alkenes

24 produced interferences ranging from $83 \pm 7\%$ for isoprene-based peroxy radicals to $96 \pm 6\%$ for

25 tetramethylethylene (TME)-based peroxy radicals, while the conversion efficiency of aromatic, aldehydes, and

26 ketone compounds ranged from $54 \pm 4\%$ for methacrolein (MACR) to $91 \pm 4\%$ for methyl vinyl ketone (MVK).

27 The RO_2 to HO_2 conversion efficiency of a number of alkanes ranged from an average measured value of $15 \pm$

28 3% for propane-based peroxy radicals to $62 \pm 4\%$ for octane-based peroxy radicals, with the RO_2 to HO_2

29 conversion efficiency increasing with the carbon number. The inlet configuration and conditions used during the

30 MCMA 2006 campaign generally resulted in lower RO_2 interferences likely due to the higher flow rate (and

31 shorter reaction time) in the detection cell and the lower NO concentration (Table 1), although the measured

conversion efficiency was found to be somewhat greater for some VOCs. Under these inlet conditions the RO_2 to HO_2 conversion efficiency for propane-based peroxy radicals was measured to be $22 \pm 11\%$ while the conversion efficiency for octane-based peroxy radicals was $30 \pm 5\%$. Because the CABINEX campaign occurred in a remote forested environment, measurements of the RO_2-to-HO_2 conversion efficiency focused on characterizing interferences from peroxy radicals produced from isoprene and its oxidation products (MVK and MACR), as isoprene peroxy radicals were predicted to contribute to more than 80% of the total RO_2 concentration during the campaign (Griffith et al., 2013). The inlet and instrumental configuration during CABINEX resulted in a higher pressure and slower sampling rate compared to the MCMA 2006 configuration. For this instrumental configuration, the RO_2-to-HO_2 conversion efficiency was found to be $91 \pm 5\%$ for isoprene-based peroxy radicals, while the conversion efficiencies for MVK and MACR were found to be $62 \pm 5\%$ and $30 \pm 7\%$, respectively.

These observations are consistent with results reported for other FAGE instruments (Fuchs et al., 2011; Whalley et al., 2011), and assumes that the photolysis of each VOC does not contribute to the production of radicals in these experiment. However, tests to determine whether photolysis of the various VOCs resulted in the formation of HO_x radicals in the absence of water vapor revealed that the photolysis of methyl vinyl ketone (MVK), methacrolein (MACR), methyl ethyl ketone (MEK), and toluene can lead to the production of HO_x radicals. The radical signals from the photolysis of methacrolein, and toluene were small and negligible relative to the total HO_x signal produced from the photolysis of water. However, the signal from the photolysis of MVK and MEK during these tests was significant and could interfere with the measurements of the RO_2-to-HO_2 conversion efficiency. These results are in contrast to that reported by Fuchs et al. (2011), who found that the photolysis of VOCs during similar tests in dry air did not produce any radicals. The reason for this discrepancy is unclear, but may be related to differences in the UV flux produced by the different mercury lamps or impurities associated with the VOC samples (Tables S1 and S2). Addition of water vapor may reduce the HO_x radical production from photolysis of these VOCs due to quenching of the excited VOC, and as a result it is difficult to quantify the interference in these experiments. However, any interference from HO_x radicals produced from the photolysis of MVK and MEK would result in higher apparent conversion efficiencies, as they could represent an additional source of HO_x radicals when the VOCs are added, and could contribute to the higher RO_2-to-HO_2 conversion efficiency reported here for MVK compared to that reported by Fuchs et al. (2011).

As previously observed, the RO_2-to-HO_2 conversion efficiency of alkene-based β-hydroxyalkyl peroxy radicals was found to be greater than the conversion efficiency of alkane-based alkyl peroxy radicals (Fuchs et al., 2011). As discussed above, this is due to due to the ability of the β-hydroxyalkoxy radicals produced from the RO_2 + NO reaction to rapidly decompose to form a hydroxyalkyl radical. The hydroxyalkyl radical reacts rapidly

1   with O_2 in the FAGE detection cell leading to the production of a carbonyl compound and HO_2. However, the

2   ability of large alkoxy radicals to rapidly isomerize and decompose (Atkinson, 1997; Finlayson-Pitts and Pitts Jr.,

3   2000) also results in a rapid production of HO_2 radicals and a larger conversion efficiency.

4   In general, reducing the reaction time in the IU-FAGE instrument reduces the conversion of these peroxy

5   radicals to HO_2, as illustrated by the reduced conversion efficiencies between the CalNex and MCMA operating

6   conditions for the majority of the VOCs tested. However, the measured conversion efficiencies of some of the

7   tested VOCs did not always display this behavior and the reasons for the discrepancies are unclear. For example,

8   the conversion efficiency for ethene peroxy radicals was lower for the CalNex configuration compared to the

9   CABINEX and MCMA configurations even though the overall flow rate was slower for the CalNex configuration.

10   However, the HO_2-to-OH conversion efficiency was also lower for this inlet configuration, suggesting that

11   reaction time may not be the only factor limiting the conversion efficiency under these instrument conditions.

12   Similarly, the conversion efficiency of MVK and MACR measured for the CABINEX instrument configuration

13   was lower than that measured for the MCMA inlet configuration, even though the overall slower flow rate in the

14   CABINEX configuration leads to a longer reaction time in the IU-FAGE detection cell. This may suggest that the

15   chemistry of peroxy radicals produced from the OH-initiated oxidation of MVK and MACR is different than that

16   of the peroxy radicals produced from the OH-initiated oxidation of alkenes and alkanes, with competing channels

17   that result in a more complex dependence on reaction time. As discussed in Fuchs et al. (2011), the fates of the

18   peroxy radicals produced by the OH initiated oxidation of MVK and MACR are not well known. For the peroxy

19   radicals produced from the OH-initiated oxidation of MVK, three decomposition channels are possible, with two

20   channels potentially leading to fast HO_2 production and one likely leading to slower HO_2 production (Fuchs et al.,

21   2011). For the peroxy radicals produced from the OH-initiated oxidation of MACR, the channel that leads to the

22   formation of a hydroxyalkyl peroxy radical likely leads to fast HO_2 production, while the channel that leads to the

23   formation of an acyl peroxy radical would lead to much slower HO_2 production (Fuchs et al., 2011).

24   **4 Discussion**

25   **4.1 RO_2 Radical Concentrations during MCMA 2006**

26   The previous analysis of the HO_2 radical concentrations during the Mexico City Metropolitan Area (MCMA)

27   2006 did not take into account interferences from RO_2 radicals (Dusanter et al., 2009b). As discussed above, the

28   instrumental conditions during MCMA-2006 resulted in the conversion of a fraction of RO_2 radicals to HO_2,

29   resulting in the measurements reflecting $HO_2^* = HO_2 + \alpha RO_2$ and overestimating the actual HO_2 concentrations.

1   To determine the fraction (α) of RO_2 radicals likely detected during the HO_2 measurements, the RO_2 radical

2   concentrations during MCMA-2006 that were previously modeled using the Regional Atmospheric Chemistry

3   Mechanism (RACM) were used to calculate the modeled HO_2* concentrations (Dusanter et al., 2009b).

4   As discussed in Dusanter et al. (2009b), the RACM model is a condensed chemical mechanism that

5   describes the gas-phase oxidation of 17 inorganic and 32 organic species. Kinetic parameters for the reactions of

6   OH, O_3 and NO_3 with inorganic species and for reactions involving organic species treated explicitly in RACM

7   (methane, ethane, ethene, formaldehyde, glyoxal, methyl peroxide and isoprene) were updated using the JPL

8   database (Sanders et al., 2006). Rate constants and branching ratios for OH, O_3 and NO_3 reactions with surrogate

9   species were used as described in the RACM model (Stockwell et al., 1997). Heterogeneous chemistry, such as

10   the incorporation of trace gases into aerosols, was not included.

11   The peroxy radical fractions calculated by the model are illustrated in Fig. 4 for 9 am, 12 pm, 6pm (local

12   times) and the overall diurnal average. Alkane-based peroxy radicals (red shades) include methyl peroxy (RACM

13   category CH3O2), ethyl peroxy (ETHP), peroxy radicals formed from the oxidation of alkanes, esters, and alkynes

14   exhibiting OH rate constants lower than 3.4×10^{-12} cm^3 $molecule^{-1}$ s^{-1} (HC3P), peroxy radicals formed from

15   alkanes, esters, and alkynes characterized by OH rate constants ranging from 3.4×10^{-12} to 6.8×10^{-12} cm^3

16    $molecule^{-1}$ s^{-1} (HC5P), and peroxy radicals formed from alkanes, esters, and alkynes whose OH rate constants are

17   larger than 6.8×10^{-12} cm^3 $molecule^{-1}$ s^{-1} (HC8P). Alkene-based peroxy radicals (blue shades) include peroxy

18   radicals from the oxidation of ethene (ETEP), external olefins (OLTP), internal olefins (OLIP), isoprene (ISOP),

19   and from α-pinene and other cyclic terpenes with one double bond (APIP). Aromatic peroxy radicals (green

20   shades) include species produced during the oxidation of toluene (TOLP), xylenes (XYLP), and cresol (CSLP).

21   The carbonyl-based peroxy radicals (grey shades) include saturated (ACO3) and unsaturated (TCO3) acyl peroxyl

22   radicals.

23   The total average modeled RO_2 concentration from 9:00 am to 6:00 pm consisted of 54% alkane-based,

24   27% alkene-based, and 14% aromatic-based peroxy radicals (Fig. 4). On average, the modeled composition of

25   peroxy radicals was relatively constant throughout the day during the MCMA campaign. The modeled relative

26   contribution of aromatic-based peroxy radicals was greater in the morning, consistent with the observed elevated

27   concentrations of benzene and toluene during the morning hours (Dusanter et al., 2009b).

28   **4.2 Implications of RO_2 interferences for HO_2 measurements during MCMA 2006**

29   The modeled diurnal average concentrations of total RO_2 radicals during MCMA is shown in Fig. 5, along with

30   the modeled HO_2 concentrations and the measured HO_2* concentrations. As discussed in Dusanter et al. (2009b),

1 the modeled HO_2 concentrations were in good agreement with the measurements during the afternoon but the

2 model underestimated the measured HO_2 concentrations during the morning hours by a factor of approximately 2

3 to 5. However, these conclusions were based on the assumption that the measured HO_2 concentrations were free

4 from interferences and could be compared to the modeled HO_2 concentrations. Based on the conversion

5 efficiencies reported for RO_2 radicals in the present study, it is clear that the MCMA measurements represent an

6 upper limit to the actual HO_2 concentrations and should be compared to the modeled $HO_2^* = HO_2 + \alpha RO_2$

7 concentrations.

8   The RACM modeled HO_2^* concentrations were calculated by applying the measured RO_2-to-HO_2

9 conversion efficiencies for the instrumental conditions reported in Table 2 for MCMA-2006 using Eq. 12:

10 $$HO_2^* = HO_2 + (0.84 \cdot ISOP + 0.68 \cdot OLIP + 0.68 \cdot OLTP + 0.86 \cdot ETEP + 0.32 \cdot TOLP + 0.32 \cdot XYLP +$$

11 $$0.32 \cdot CSLP + 0.72 \cdot APIP + 0.22 \cdot HC3P + 0.22 \cdot HC5P + 0.30 \cdot HC8P + 0.05 \cdot CH3O2 + 0.07 \cdot ETHP$$

12 $$+ 0.32 \cdot ACO3 + 0.32 \cdot TCO3 + 0.72 \cdot KETP \tag{12}$$

13 The contribution for isoprene peroxy radicals (ISOP), ethene peroxy radicals (ETEP), and toluene peroxy radicals

14 (TOLP) were taken directly from Table 2. The average RO_2-to-HO_2 conversion efficiency for *trans*-2-butene and

15 tetramethylethelene-based peroxy radicals was used for the conversion efficiency of peroxy radicals from internal

16 olefins (OLIP), and external olefins (OLTP), while the conversion efficiency for *trans*-2-butene was used for the

17 conversion efficiency for α-pinene and other cyclic terpene peroxy radicals (APIP). The measured conversion

18 efficiency for toluene-based peroxy radicals was used to represent the conversion efficiency for xylene (XYLP)

19 and cresol (CSLP) peroxy radicals. The conversion efficiency of methacrolein-based peroxy radicals was used to

20 represent the conversion efficiency of acetyl peroxy and higher saturated acyl peroxy radicals (ACO3) as well as

21 unsaturated acyl peroxy radicals (TCO3), while the conversion efficiency of methyl vinyl ketone-based peroxy

22 radicals was used to represent the efficiency of ketone-based peroxy radicals (KETP).

23   The overall average contribution of peroxy radicals to the modeled HO_2^* and the relative contribution of

24 each RACM peroxy radical category to the RO_2 interference are shown in Fig. 6. Because the HO_2-to-OH

25 conversion efficiency of 80% in these experiments was approximately 20% lower than the conversion efficiency

26 measured during the campaign (Dusanter et al., 2008; Dusanter et al., 2009a), the relative peroxy radical

27 contributions illustrated in this figure are likely lower limits to the actual contribution during the campaign.

28   On average, RO_2 radicals contributed to approximately 35% of the total modeled HO_2^* (Fig. 6). While

29 alkanes compose the majority of the modeled peroxy radicals (Fig. 4), they only contributed to about 29% of the

30 RO_2 interference, while alkenes contributed to approximately 51% to the interference (Fig. 6). While isoprene

1   peroxy radicals contributed to only 5% of the total RO_2 concentration, they contributed approximately 11% to the

2   interference.

3   The overall contribution of RO_2 radicals to the measured HO_2* concentrations in this environment is

4   similar to that observed during the CalNex campaign, where RO_2 radicals were modeled to contribute to

5   approximately 30% of the measured HO_2* concentrations, although during CalNex peroxy radicals from isoprene

6   (ISOP) and its oxidation products accounted for approximately 40-50% of the modeled interference and olefins

7   (OLTP, OLIP) contributed approximately 20-30% (Griffith et al., 2016). Unlike these urban environments, in

8   forested environments where the OH reactivity is dominated by isoprene and other unsaturated biogenic

9   emissions, isoprene and other biogenic hydroxyl alkyl peroxy radicals can be the dominant peroxy radicals and

10   can make a significant contribution to the measured HO_2* concentrations due to their high conversion efficiency

11   to HO_2 in the FAGE detection cell (Table 2). For example, during the CABINEX campaign in a northern Michigan

12   forest, isoprene peroxy radicals were modeled to be the dominant peroxy radical in this environment and the main

13   contributor to the interference, contributing to approximately 50% of the modeled HO_2* concentrations during

14   the daytime (Griffith et al., 2013). As a result, previous measurements of HO_2 in these environments by LIF-

15   FAGE or other chemical conversion techniques are likely influenced by an interference from β-hydroxyalkyl

16   peroxy radicals such as those produced by the OH-initiated oxidation of isoprene and other biogenic emissions.

17   While it is possible to subtract the modeled speciated RO_2 concentrations from the measured HO_2* and compare

18   the results to the modeled HO_2, this method increases the uncertainty associated with the measured concentrations

19   due to the additional uncertainty associated with the modeled RO_2 concentrations as well as the uncertainties

20   associated with the measured RO_2–to-HO_2 conversion efficiencies. We estimate the uncertainty associated with

21   the RACM modeled RO_2 to be approximately ±70% (2σ), similar to that for the modeled HO_2 (Dusanter et al.,

22   2009b). As a result, we prefer to compare the modeled HO_2* to the measured HO_2*.

23   The diurnal average modeled HO_2* concentrations for the MCMA-2006 campaign are also shown in Fig.

24   5. As can be seen in this figure, the model overestimates the measured HO_2* by approximately 35% between

25   12:00 and 17:00 CST, although the modeled results are generally close to the upper bound of the calibration

26   accuracy (36%, 2σ) (Dusanter et al., 2009b). As discussed above, the modeled HO_2* is likely a lower limit given

27   that the RO_2-to-HO_2 conversion efficiencies during the campaign may be greater than shown in Table 2 due to the

28   higher HO_2-to-OH conversion efficiency measured during the campaign. Although, the measured HO_2* are still

29   likely to be within the overall uncertainty of the model, which was estimated to be approximately a factor of 1.7

30   (Dusanter et al., 2009b), these results suggest that the model likely overestimates the measured concentrations

31   during the afternoon.

1   These results are in contrast to the results from the CalNex campaign, where the simulations using the

2 RACM2 model tended to underestimate the measured HO_2* concentrations during the week, when NO mixing

3 ratios were greater than 4 ppb (Griffith et al., 2016). The reason for this difference between the campaigns is

4 unclear, but may be related to the relative concentrations of dicarbonyl species and their treatment in the RACM

5 and RACM2 models. Dusanter et al. (2009b) demonstrated that the RACM model results for MCMA-2006 were

6 highly sensitive to the concentrations of dicarbonyl species in the model, with the model significantly

7 overpredicting the concentration of HO_x radicals when unmeasured concentrations of these species were not

8 constrained. Daytime average measured glyoxal mixing ratios during MCMA-2006 were approximately 0.4 ppb

9 (Dusanter et al., 2009b), which were greater than the maximum daytime mixing ratios of 0.16 ppb during CalNex

10 (Washenfelder et al., 2011), suggesting that the MCMA-2006 results may be more sensitive to the treatment of

11 dicarbonyl chemistry compared to CalNex. Additional analysis and modeling will be needed to resolve this issue.

12   While the model tends to overestimate the measured HO_2* concentrations during the afternoon, it

13 underestimates the measured HO_2* concentrations in the morning by a factor of 3 between 9-11 am. As discussed

14 in Dusanter et al. (2009b), this may suggest that a significant radical source may be missing from current

15 atmospheric models under polluted conditions. Similar results were observed in Wangdu, China by Tan et al.

16 (2017). In this study, total peroxy radical concentrations were measured by chemical conversion to HO_2 in an

17 external reactor with subsequent detection of HO_2 (after chemical conversion to OH) in an LIF-FAGE instrument.

18 They also measured HO_2 radicals using a second LIF-FAGE detection axis that minimized interferences from

19 RO_2 radicals. They found that a model using the updated RACM2 mechanism was able to reproduce the observed

20 HO_2 concentrations during the day, but underestimated the observed total RO_2 concentration by a factor of 3 to 5

21 in the morning when NO concentrations were higher than 1 ppbv. The observed RO_2 concentrations could be

22 explained by a missing RO_2 source of 2 ppbv h^{-1} (Tan et al., 2017).

23   Dusanter et al. (2009b) also compared the measured HO_2*/OH ratio to the RACM modeled HO_2/OH

24 ratio and found that the model underpredicted the observed ratio, especially under conditions where the mixing

25 ratio of NO was greater than 5 ppb. At NO mixing ratios of 10 ppb, the model underestimated the measured ratio

26 by a factor of 2 (Dusanter et al., 2009b). However, comparing the measured HO_2*/OH ratio to the modeled

27 HO_2*/OH ratio improves the agreement even though the model tends to overpredict both OH and HO_2* in the

28 afternoon (Fig. 7). This may indicate that there is either a missing sink of HO_x radicals in the model or a

29 miscalculation of the relative rates of initiation and/or termination. At an NO mixing ratio of 10 ppb the modeled

30 HO_2*/OH ratio is in good agreement with the measurements, although it still underestimates the measured

31 HO_2*/OH ratio at higher NO mixing ratios by as much as a factor of 4, and may also overestimate the HO_2*/OH

1 ratio for mixing ratios of NO less than 5 ppb by as much as a factor of 2 (Fig. 7). It is interesting to note that a

2 model underestimation of the total OH reactivity at high NO mixing ratios may contribute to this discrepancy.

3 Unfortunately, total OH reactivity was not measured during MCMA-2006 and the reliability of the model to

4 simulate it could not be assessed. Similar results were observed for the CalNex campaign (Griffith et al., 2016),

5 which included direct measurements of the total OH reactivity. Although accounting for the missing reactivity in

6 the analysis of the CalNex data improved the agreement between the measured and modeled HO_2^*/OH ratio, the

7 model still underestimates the measured ratio at high mixing ratios of NO (Griffith et al., 2016). These results

8 suggest that our understanding of the radical propagation chemistry under high NO conditions may be incomplete.

9 **5. Summary and Conclusions**

10 The RO_2 interference associated with measurements of HO_2 by the IU-FAGE instrument was

11 characterized for three different instrument configurations that were used in previous field campaigns (MCMA

12 2006, CABINEX 2009, and CalNex 2010). Similar to that reported for other LIF-FAGE instruments, the RO_2-to-

13 HO_2 conversion efficiency was highest for alkene- and aromatic-based RO_2 radicals, producing higher levels of

14 interference, while the conversion efficiency of alkane-based RO_2 radicals was less but increased with increasing

15 carbon number. In general, the conversion efficiency was higher for instrument configurations that involved

16 slower sampling flow rates and longer reaction times between the peroxy radicals and NO in the detection cell.

17 The similarities in the measured RO_2 conversion efficiencies reported here with those reported for other

18 LIF-FAGE instruments suggest that the main factor controlling the conversion efficiency is the rate of reaction of

19 RO_2 radicals with NO, and that increasing the efficiency of the conversion of HO_2 to OH will also increases the

20 RO_2-to-HO_2 conversion efficiency. Although the impact of differences in the characteristics of the low pressure

21 expansion in LIF-FAGE instruments cannot be ruled out, these results suggest that the interferences reported here

22 associated with measurements of HO_2 are likely similar for all instruments that measure HO_2 by chemical

23 conversion through reaction with NO. Previous measurements of HO_2 radicals by instruments using this method

24 were likely influenced by the conversion of RO_2 radicals, with measurements of HO_2 in forested environments

25 likely influenced by interferences from peroxy radicals derived from biogenic alkenes such as isoprene due to the

26 high RO_2-to-HO_2 conversion efficiencies of these radicals. Because of the lower conversion efficiencies of alkane-

27 based peroxy radicals, the impact on previous measurements in urban areas will depend on the relative

28 concentrations of alkanes versus alkenes and aromatics contributing to the overall pool of peroxy radicals in these

29 environments.

While this interference was taken into account to investigate the radical chemistry during CABINEX (Griffith et al., 2013) and CalNex (Griffith et al., 2016), this issue was not known when the radical measurements from the MCMA-2006 field campaign were published (Dusanter et al., 2009b). An analysis of the impact of this interference on the results for the MCMA-2006 campaign suggests that the RO_2 radical contribution to the measured HO_2* concentration was approximately 35% based on the RACM modeled RO_2 concentrations. Taking this interference into account, the resulting modeled HO_2* concentrations were generally greater than the measured concentrations by 35% during the afternoon, although the model results were within the calibration uncertainty of the measurements (36% at 2σ). Given that the modeled HO_2* concentrations likely reflect a lower limit to the interference during the campaign these results suggest that the model likely overestimates the measured concentrations during the afternoon. However, the model still underestimates the HO_2* concentration by a factor of 3 in the morning, suggesting that the model may be missing an important radical source in the morning. Although the measured HO_2*/OH ratio was in better agreement with the modeled HO_2*/OH ratio compared to the modeled HO_2/OH ratio, the model still significantly underestimates the HO_2*/OH ratio by up to a factor of 4 for NO mixing ratios greater than 10 ppb, suggesting that our understanding of radical propagation under these conditions is still incomplete.

Future measurements of peroxy radicals by the IU-FAGE instrument will involve measurements at lower NO concentrations to minimize the RO_2-to-HO_2 conversion efficiency. Recent experiments have demonstrated that the addition of an NO concentration of approximately 9×10^{11} cm^{-3} results in an HO_2-to-OH conversion efficiency of approximately 17% and a conversion efficiency of isoprene-based peroxy radicals to HO_2 of approximately 10%. Even at this low HO_2-to-OH conversion efficiency, the resulting HO_2 signals are still significantly greater than the limit of detection of the instrument, but at this low NO concentration, the subsequent conversion of isoprene peroxy radicals to OH is negligible, allowing for measurements of ambient HO_2 concentrations without interferences from RO_2 radicals.

Acknowledgements. This work was supported by grants from the National Science Foundation (AGS-1104880 and AGS-1440834) and the National Aeronautics and Space Administration (NNX12AE55G). We would also like to thank Stephen Griffith for his helpful insights during the early stages of this project and Jennifer Liljegren for experimental assistance.

References

Atkinson, R.: Atmospheric reactions of alkoxy and β-hydroxyalkoxy radicals, Int. J. Chem. Kinet., 29, 99-111, 1997.

Cantrell, C. A., Zimmer, A., and Tyndall, G. S.: Absorption cross sections for water vapor from 183 to 193 nm, Geophysical Research Letters, 24, 2195-2198, 1997.

Carslaw, N., Creasey, D. J., Harrison, D., Heard, D. E., Hunter, M. C., Jacobs, P. J., Jenkin, M. E., Lee, J. D., Lewis, A. C., Pilling, M. J., Saunders, S. M., and Seakins, P. W.: OH and HO_2 radical chemistry in a forested region of north-western Greece, Atmospheric Environment, 35, 4725-4737, 2001.

Chen, S., Ren, X., Mao, J., Chen, Z., Brune, W. H., Lefer, B., Rappenglück, B., Flynn, J., Olson, J., and Crawford, J. H.: A comparison of chemical mechanisms based on TRAMP-2006 field data, Atmospheric Environment, 44, 4116-4125, 2010.

Creasey, D. J., Heard, D. E., and Lee, J. D.: Absorption cross-section measurements of water vapour and oxygen at 185 nm. Implications for the calibration of field instruments to measure OH, HO_2 and RO_2 radicals, Geophysical Research Letters, 27, 1651-1654, 2000.

Creasey, D. J., Heard, D. E., and Lee, J. D.: Eastern Atlantic Spring Experiment 1997 (EASE97) 1. Measurements of OH and HO_2 concentrations at Mace Head, Ireland, Journal of Geophysical Research: Atmospheres, 107, 4091, 4010.1029/2001JD000892, 2002.

Czader, B. H., Li, X., and Rappenglueck, B.: CMAQ modeling and analysis of radicals, radical precursors, and chemical transformations, J. Geophys. Res., 118, 11,376-311,387, 2013.

Dusanter, S., Vimal, D., and Stevens, P. S.: Technical note: Measuring tropospheric OH and HO_2 by laser-induced fluorescence at low pressure. A comparison of calibration techniques, Atmos. Chem. Phys., 8, 321-340, 2008.

Dusanter, S., Vimal, D., Stevens, P. S., Volkamer, R., and Molina, L. T.: Measurements of OH and HO_2 concentrations during the MCMA-2006 field campaign – Part 1: Deployment of the Indiana University laser-induced fluorescence instrument, Atmos. Chem. Phys., 9, 1665-1685, 2009a.

Dusanter, S., Vimal, D., Stevens, P. S., Volkamer, R., Molina, L. T., Baker, A., Meinardi, S., Blake, D., Sheehy, P., Merten, A., Zhang, R., Zheng, J., Fortner, E. C., Junkermann, W., Dubey, M., Rahn, T., Eichinger, B., Lewandowski, P., Prueger, J., and Holder, H.: Measurements of OH and HO_2 concentrations during the MCMA-2006 field campaign – Part 2: Model comparison and radical budget, Atmos. Chem. Phys., 9, 6655-6675, 2009b.

Emmerson, K. M., Carslaw, N., Carpenter, L. J., Heard, D. E., Lee, J. D., and Pilling, M. J.: Urban Atmospheric Chemistry During the PUMA Campaign 1: Comparison of Modelled OH and HO_2 Concentrations with Measurements, J Atmos Chem, 52, 143-164, 2005.

Emmerson, K. M., Carslaw, N., Carslaw, D. C., Lee, J. D., McFiggans, G., Bloss, W. J., Gravestock, T., Heard, D. E., Hopkins, J., Ingham, T., Pilling, M. J., Smith, S. C., Jacob, M., and Monks, P. S.: Free radical modelling studies during the UK TORCH Campaign in Summer 2003, Atmos. Chem. Phys., 7, 167-181, 2007.

Finlayson-Pitts, B. J., and Pitts Jr., J. N.: Chemistry of the Upper and Lower Atmosphere, Academic Press, San Diego, 2000.

Fuchs, H., Brauers, T., Dorn, H. P., Harder, H., Häseler, R., Hofzumahaus, A., Holland, F., Kanaya, Y., Kajii, Y., Kubistin, D., Lou, S., Martinez, M., Miyamoto, K., Nishida, S., Rudolf, M., Schlosser, E., Wahner, A., Yoshino, A., and Schurath, U.: Technical Note: Formal blind intercomparison of HO_2 measurements in the atmosphere simulation chamber SAPHIR during the HOxComp campaign, Atmos. Chem. Phys., 10, 12233-12250, 2010.

Fuchs, H., Bohn, B., Hofzumahaus, A., Holland, F., Lu, K. D., Nehr, S., Rohrer, F., and Wahner, A.: Detection of HO_2 by laser-induced fluorescence: calibration and interferences from RO_2 radicals, Atmos. Meas. Tech., 4, 1209-1225, 2011.

George, L. A., Hard, T. M., and O'Brien, R. J.: Measurement of free radicals OH and HO_2 in Los Angeles smog, Journal of Geophysical Research: Atmospheres, 104, 11643-11655, 1999.

Griffith, S. M., Hansen, R. F., Dusanter, S., Stevens, P. S., Alaghmand, M., Bertman, S. B., Carroll, M. A., Erickson, M., Galloway, M., Grossberg, N., Hottle, J., Hou, J., Jobson, B. T., Kammrath, A., Keutsch, F. N., Lefer, B. L., Mielke, L. H., O'Brien, A., Shepson, P. B., Thurlow, M., Wallace, W., Zhang, N., and Zhou, X. L.: OH and HO_2 radical chemistry during PROPHET 2008 and CABINEX 2009 - Part 1: Measurements and model comparison, Atmos. Chem. Phys., 13, 5403-5423, 2013.

Griffith, S. M., Hansen, R. F., Dusanter, S., Michoud, V., Gilman, J. B., Kuster, W. C., Veres, P. R., Graus, M., de Gouw, J. A., Roberts, J., Young, C., Washenfelder, R., Brown, S. S., Thalman, R., Waxman, E., Volkamer, R., Tsai, C., Stutz, J., Flynn, J. H., Grossberg, N., Lefer, B., Alvarez, S. L., Rappenglueck, B., Mielke, L. H., Osthoff, H. D., and Stevens, P. S.: Measurements of hydroxyl and hydroperoxy radicals during CalNex-LA: Model comparisons and radical budgets, Journal of Geophysical Research: Atmospheres, 121, 4211-4232, 2016.

Heard, D. E., and Pilling, M. J.: Measurement of OH and HO_2 in the troposphere, Chemical Reviews, 103, 5163-5198, 2003.

Hens, K., Novelli, A., Martinez, M., Auld, J., Axinte, R., Bohn, B., Fischer, H., Keronen, P., Kubistin, D., Nölscher, A. C., Oswald, R., Paasonen, P., Petäjä, T., Regelin, E., Sander, R., Sinha, V., Sipilä, M., Taraborrelli, D., Tatum Ernest, C., Williams, J., Lelieveld, J., and Harder, H.: Observation and modelling of HO_x radicals in a boreal forest, Atmos. Chem. Phys., 14, 8723-8747, 2014.

Hofzumahaus, A., Brauers, T., Aschmutat, U., Brandenburger, U., Dorn, H. P., Hausmann, M., Heßling, M., Holland, F., Plass-Dülmer, C., Sedlacek, M., Weber, M., and Ehhalt, D. H.: Reply to "Comment on 'The measurement of tropospheric OH radicals by laser-induced fluorescence spectroscopy during the POPCORN field campaign' by Hofzumahaus et al. and 'Intercomparison of tropospheric OH radical measurements by multiple folded long-path laser absorption and laser induced fluorescence' by Brauers et al.", Geophysical Research Letters, 24, 3039-3040, 1997.

Holland, F., Hofzumahaus, A., Schäfer, J., Kraus, A., and Pätz, H.-W.: Measurements of OH and HO_2 radical concentrations and photolysis frequencies during BERLIOZ, Journal of Geophysical Research: Atmospheres, 108, 8246, doi:8210.1029/2001JD001393, 2003.

Kanaya, Y., Sadanaga, Y., Hirokawa, J., Kajii, Y., and Akimoto, H.: Development of a Ground-Based LIF Instrument for Measuring HOx Radicals: Instrumentation and Calibrations, J Atmos Chem, 38, 73-110, 2001.

Kanaya, Y., Cao, R., Akimoto, H., Fukuda, M., Komazaki, Y., Yokouchi, Y., Koike, M., Tanimoto, H., Takegawa, N., and Kondo, Y.: Urban photochemistry in central Tokyo: 1. Observed and modeled OH and HO_2 radical concentrations during the winter and summer of 2004, Journal of Geophysical Research: Atmospheres, 112, doi:10.1029/2007JD008670, 2007a.

Kanaya, Y., Cao, R., Kato, S., Miyakawa, Y., Kajii, Y., Tanimoto, H., Yokouchi, Y., Mochida, M., Kawamura, K., and Akimoto, H.: Chemistry of OH and HO_2 radicals observed at Rishiri Island, Japan, in September 2003: Missing daytime sink of HO_2 and positive nighttime correlations with monoterpenes, Journal of Geophysical Research: Atmospheres, 112, doi:10.1029/2006JD007987, 2007b.

Kanaya, Y., Hofzumahaus, A., Dorn, H. P., Brauers, T., Fuchs, H., Holland, F., Rohrer, F., Bohn, B., Tillmann, R., Wegener, R., Wahner, A., Kajii, Y., Miyamoto, K., Nishida, S., Watanabe, K., Yoshino, A., Kubistin, D., Martinez, M., Rudolf, M., Harder, H., Berresheim, H., Elste, T., Plass-Dülmer, C., Stange, G., Kleffmann, J., Elshorbany, Y., and Schurath, U.: Comparisons of observed and modeled

OH and HO_2 concentrations during the ambient measurement period of the HOxComp field campaign, Atmos. Chem. Phys., 12, 2567-2585, 2012.

Kim, S., Wolfe, G. M., Mauldin, L., Cantrell, C., Guenther, A., Karl, T., Turnipseed, A., Greenberg, J., Hall, S. R., Ullmann, K., Apel, E., Hornbrook, R., Kajii, Y., Nakashima, Y., Keutsch, F. N., DiGangi, J. P., Henry, S. B., Kaser, L., Schnitzhofer, R., Graus, M., Hansel, A., Zheng, W., and Flocke, F. F.: Evaluation of HO_x sources and cycling using measurement-constrained model calculations in a 2-methyl-3-butene-2-ol (MBO) and monoterpene (MT) dominated ecosystem, Atmos. Chem. Phys., 13, 2031-2044, 2013.

Klotz, B., Sørensen, S., Barnes, I., Becker, K. H., Etzkorn, T., Volkamer, R., Platt, U., Wirtz, K., and Martín-Reviejo, M.: Atmospheric Oxidation of Toluene in a Large-Volume Outdoor Photoreactor: In Situ Determination of Ring-Retaining Product Yields, The Journal of Physical Chemistry A, 102, 10289-10299, 1998.

Konrad, S., Schmitz, T., Buers, H. J., Houben, N., Mannschreck, K., Mihelcic, D., Müsgen, P., Pätz, H. W., Holland, F., Hofzumahaus, A., Schäfer, H. J., Schröder, S., Volz-Thomas, A., Bächmann, K., Schlomski, S., Moortgat, G., and Großmann, D.: Hydrocarbon measurements at Pabstthum during the BERLIOZ campaign and modeling of free radicals, J. Geophys. Res., 108, 8251, 2003.

Kubistin, D., Harder, H., Martinez, M., Rudolf, M., Sander, R., Bozem, H., Eerdekens, G., Fischer, H., Gurk, C., Klüpfel, T., Königstedt, R., Parchatka, U., Schiller, C. L., Stickler, A., Taraborrelli, D., Williams, J., and Lelieveld, J.: Hydroxyl radicals in the tropical troposphere over the Suriname rainforest: comparison of measurements with the box model MECCA, Atmos. Chem. Phys., 10, 9705-9728, 2010.

Lanzendorf, E. J., Hanisco, T. F., Donahue, N. M., and Wennberg, P. O.: Comment on: "The measurement of tropospheric OH radicals by laser-induced fluorescence spectroscopy during the POPCORN Field Campaign" by Hofzumahaus et al. and "Intercomparison of tropospheric OH radical measurements by multiple folded long-path laser absorption and laser induced fluorescence" by Brauers et al, Geophysical Research Letters, 24, 3037-3038, 1997.

Levy, H.: Photochemistry of the lower troposphere, Planetary and Space Science, 20, 919-935, 1972.

Lu, K. D., Hofzumahaus, A., Holland, F., Bohn, B., Brauers, T., Fuchs, H., Hu, M., Häseler, R., Kita, K., Kondo, Y., Li, X., Lou, S. R., Oebel, A., Shao, M., Zeng, L. M., Wahner, A., Zhu, T., Zhang, Y. H., and Rohrer, F.: Missing OH source in a suburban environment near Beijing: observed and modelled OH and HO_2 concentrations in summer 2006, Atmos. Chem. Phys., 13, 1057-1080, 2013.

Mao, J., Ren, X., Zhang, L., Van Duin, D. M., Cohen, R. C., Park, J. H., Goldstein, A. H., Paulot, F., Beaver, M. R., Crounse, J. D., Wennberg, P. O., DiGangi, J. P., Henry, S. B., Keutsch, F. N., Park, C., Schade, G. W., Wolfe, G. M., Thornton, J. A., and Brune, W. H.: Insights into hydroxyl measurements and atmospheric oxidation in a California forest, Atmos. Chem. Phys., 12, 8009-8020, 2012.

Martinez, M., Harder, H., Kovacs, T. A., Simpas, J. B., Bassis, J., Lesher, R., Brune, W. H., Frost, G. J., Williams, E. J., Stroud, C. A., Jobson, B. T., Roberts, J. M., Hall, S. R., Shetter, R. E., Wert, B., Fried, A., Alicke, B., Stutz, J., Young, V. L., White, A. B., and Zamora, R. J.: OH and HO_2 concentrations, sources, and loss rates during the Southern Oxidants Study in Nashville, Tennessee, summer 1999, Journal of Geophysical Research: Atmospheres, 108, n/a-n/a, 2003.

Michoud, V., Kukui, A., Camredon, M., Colomb, A., Borbon, A., Miet, K., Aumont, B., Beekmann, M., Durand-Jolibois, R., Perrier, S., Zapf, P., Siour, G., Ait-Helal, W., Locoge, N., Sauvage, S., Afif, C., Gros, V., Furger, M., Ancellet, G., and Doussin, J. F.: Radical budget analysis in a suburban European site during the MEGAPOLI summer field campaign, Atmos. Chem. Phys., 12, 11951-11974, 2012.

Nehr, S., Bohn, B., Fuchs, H., Hofzumahaus, A., and Wahner, A.: HO_2 formation from the OH + benzene reaction in the presence of O_2, Physical Chemistry Chemical Physics, 13, 10699-10708, 2011.

Okabe, H.: Photochemistry of small molecules, John Wiley & Sons, New York, 1978.

Ren, X., Harder, H., Martinez, M., Lesher, R. L., Oliger, A., Simpas, J. B., Brune, W. H., Schwab, J. J., Demerjian, K. L., He, Y., Zhou, X., and Gao, H.: OH and HO_2 Chemistry in the urban atmosphere of New York City, Atmospheric Environment, 37, 3639-3651, 2003.

Ren, X., Brune, W., Cantrell, C., Edwards, G., Shirley, T., Metcalf, A., and Lesher, R.: Hydroxyl and Peroxy Radical Chemistry in a Rural Area of Central Pennsylvania: Observations and Model Comparisons, J Atmos Chem, 52, 231-257, 2005.

Ren, X., Brune, W. H., Oliger, A., Metcalf, A. R., Simpas, J. B., Shirley, T., Schwab, J. J., Bai, C., Roychowdhury, U., Li, Y., Cai, C., Demerjian, K. L., He, Y., Zhou, X., Gao, H., and Hou, J.: OH, HO_2, and OH reactivity during the PMTACS–NY Whiteface Mountain 2002 campaign: Observations and model comparison, Journal of Geophysical Research: Atmospheres, 111, doi:10.1029/2005JD006126, 2006.

Ren, X., van Duin, D., Cazorla, M., Chen, S., Mao, J., Zhang, L., Brune, W. H., Flynn, J. H., Grossberg, N., Lefer, B. L., Rappenglück, B., Wong, K. W., Tsai, C., Stutz, J., Dibb, J. E., Thomas Jobson, B., Luke, W. T., and Kelley, P.: Atmospheric oxidation chemistry and ozone production: Results from SHARP 2009 in Houston, Texas, Journal of Geophysical Research: Atmospheres, 118, 5770-5780, 2013.

Rohrer, F., Lu, K., Hofzumahaus, A., Bohn, B., Brauers, T., Chang, C.-C., Fuchs, H., Haseler, R., Holland, F., Hu, M., Kita, K., Kondo, Y., Li, X., Lou, S., Oebel, A., Shao, M., Zeng, L., Zhu, T., Zhang, Y., and Wahner, A.: Maximum efficiency in the hydroxyl-radical-based self-cleansing of the troposphere, Nature Geosci, 7, 559-563, 2014.

Sanders, S. P., Friedl, R. R., Golden, D. M., Kurylo, M. J., Moortgat, G. K., Wine, P. H., Ravishankara, A. R., Kolb, C. E., Molina, M. J., Finlayson-Pitts, B. J., Huie, R. E., and Orkin, V. L.: Chemical Kinetics and photochemical data for use in atmospheric studies, Evaluation Number 15, JPL Publications 06-2, 2006.

Sheehy, P. M., Volkamer, R., Molina, L. T., and Molina, M. J.: Oxidative capacity of the Mexico City atmosphere – Part 2: A RO_x radical cycling perspective, Atmos. Chem. Phys., 10, 6993-7008, 2010.

Shirley, T. R., Brune, W. H., Ren, X., Mao, J., Lesher, R., Cardenas, B., Volkamer, R., Molina, L. T., Molina, M. J., Lamb, B., Velasco, E., Jobson, T., and Alexander, M.: Atmospheric oxidation in the Mexico City Metropolitan Area (MCMA) during April 2003, Atmos. Chem. Phys., 6, 2753-2765, 2006.

Stevens, P. S., Mather, J. H., and Brune, W. H.: Measurement of tropospheric OH and HO_2 by laser-induced fluorescence at low pressure, J. Geophys. Res., 99, 3543-3557, 1994.

Stockwell, W. R., Kirchner, F., Kuhn, M., and Seefeld, S.: A new mechanism for regional atmospheric chemistry modeling, Journal of Geophysical Research: Atmospheres, 102, 25847-25879, 1997.

Tan, D., Faloona, I., Simpas, J. B., Brune, W., Shepson, P. B., Couch, T. L., Sumner, A. L., Carroll, M. A., Thornberry, T., Apel, E., Riemer, D., and Stockwell, W.: HO_x budgets in a deciduous forest: Results from the PROPHET summer 1998 campaign, Journal of Geophysical Research: Atmospheres, 106, 24407-24427, 2001.

Tan, Z., Fuchs, H., Lu, K., Bohn, B., Broch, S., Dong, H., Gomm, S., Haeseler, R., He, L., Hofzumahaus, A., Holland, F., Li, X., Liu, Y., Lu, S., Rohrer, F., Shao, M., Wang, B., Wang, M., Wu, Y., Zeng, L., Zhang, Y., Wahner, A., and Zhang, Y.: Radical chemistry at a rural site (Wangdu) in the North China Plain: Observation and model calculations of OH, HO_2 and RO_2 radicals, Atmos. Chem. Phys., 17, 663-690, 2017.

Washenfelder, R. A., Young, C. J., Brown, S. S., Angevine, W. M., Atlas, E. L., Blake, D. R., Bon, D. M., Cubison, M. J., de Gouw, J. A., Dusanter, S., Flynn, J., Gilman, J. B., Graus, M., Griffith, S., Grossberg, N., Hayes, P. L., Jimenez, J. L., Kuster, W. C., Lefer, B. L., Pollack, I. B., Ryerson, T. B., Stark, H., Stevens, P. S., and Trainer, M. K.: The glyoxal budget and its contribution to organic aerosol

for Los Angeles, California, during CalNex 2010, Journal of Geophysical Research: Atmospheres, 116, doi:10.1029/2011JD016314, 2011.

Whalley, L. K., Edwards, P. M., Furneaux, K. L., Goddard, A., Ingham, T., Evans, M. J., Stone, D., Hopkins, J. R., Jones, C. E., Karunaharan, A., Lee, J. D., Lewis, A. C., Monks, P. S., Moller, S. J., and Heard, D. E.: Quantifying the magnitude of a missing hydroxyl radical source in a tropical rainforest, Atmos. Chem. Phys., 11, 7223-7233, 2011.

Whalley, L. K., Blitz, M. A., Desservettaz, M., Seakins, P. W., and Heard, D. E.: Reporting the sensitivity of laser-induced fluorescence instruments used for HO_2 detection to an interference from RO_2 radicals and introducing a novel approach that enables HO_2 and certain RO_2 types to be selectively measured, Atmos. Meas. Tech., 6, 3425-3440, 2013.

Table 1. Configuration of the IU-FAGE instrument during various previous field campaigns.

	CalNex	CABINEX	MCMA-2006
Cell pressure (hPa)	5.5	10.0	7.2
Orifice diameter (mm)	0.64	1.02	1.02
Sample flow rate (SLPM)	3.4	8.5	10
NO (molecules/cm^3) (for 1 sccm flow)	2.9×10^{13}	2.1×10^{13}	1.3×10^{13}

Table 2. Average measured f $_{RO2 \rightarrow HO2}$ for various alkenes and alkanes under different inlet conditions. Uncertainties represents the standard error of the mean from all individual experiments, with the number of experiments shown in parentheses.

Compounds	4 Torr @ 3.4 SLPM (CalNex)	7.5 Torr @ 8.5 SLPM (CABINEX)	5 Torr @ 10 SLPM (MCMA 2006)	Fuchs et al.[a]	Whalley et al.[b]
C(HO$_2$→OH)	0.67 ± 0.01 (67)	0.90 ± 0.02 (47)	0.80 ± 0.01 (81)	—	—
Isoprene	0.83 ± 0.07 (5)	0.91 ± 0.05 (9)	0.84 ± 0.05 (6)	0.79 ± 0.05	0.92 ± 0.04
MVK	0.91 ± 0.04 (10)	0.62 ± 0.05 (21)	0.72 ± 0.04 (15)	0.60 ± 0.06	—
MACR	0.54 ± 0.04 (4)	0.30 ± 0.07 (5)	0.32 ± 0.07 (11)	0.58 ± 0.17	—
MEK	0.57 ± 0.06 (6)	0.62 ± 0.01 (2)	0.51 ± 0.07 (9)	—	—
Ethene	0.65 ± 0.05 (18)	0.81 ± 0.06 (7)	0.86 ± 0.06 (9)	0.85 ± 0.05	1.00 ± 0.08
trans-2-butene	0.92 ± 0.04 (4)	—	0.72 ± 0.03 (6)	—	—
TME	0.96 ± 0.06 (2)	—	0.64 ± 0.06 (8)	—	—
Toluene	0.65 ± 0.07 (4)	—	0.32 ± 0.10 (6)	—	—
Propane	0.15 ± 0.03 (4)	—	0.22 ± 0.11 (2)	—	0.03 ± 0.01
n-butane	0.31 ± 0.03 (4)	0.30 ± 0.03 (3)	0.23 ± 0.05 (4)	—	0.18 ± 0.01
n-octane	0.62 ± 0.04 (5)	—	0.30 ± 0.05 (5)	—	—

[a]Fraction of conversion for RO$_2$ to HO$_2$ conversion for the Julich LIF instrument (Fuchs et al., 2011)
[b] Conversion efficiencies of RO$_2$ to OH for the Leeds LIF instrument referenced to ethene (Whalley et al., 2013)
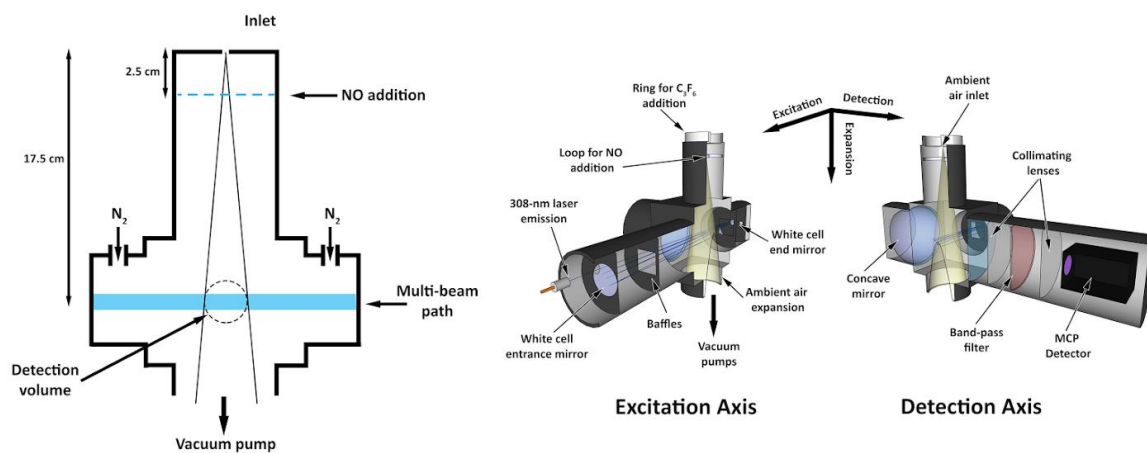
Figure 1. Indiana University LIF-FAGE cross section (left) and a schematic of the sampling/excitation axis and the sampling detection axis (right) (Dusanter et al., 2008)
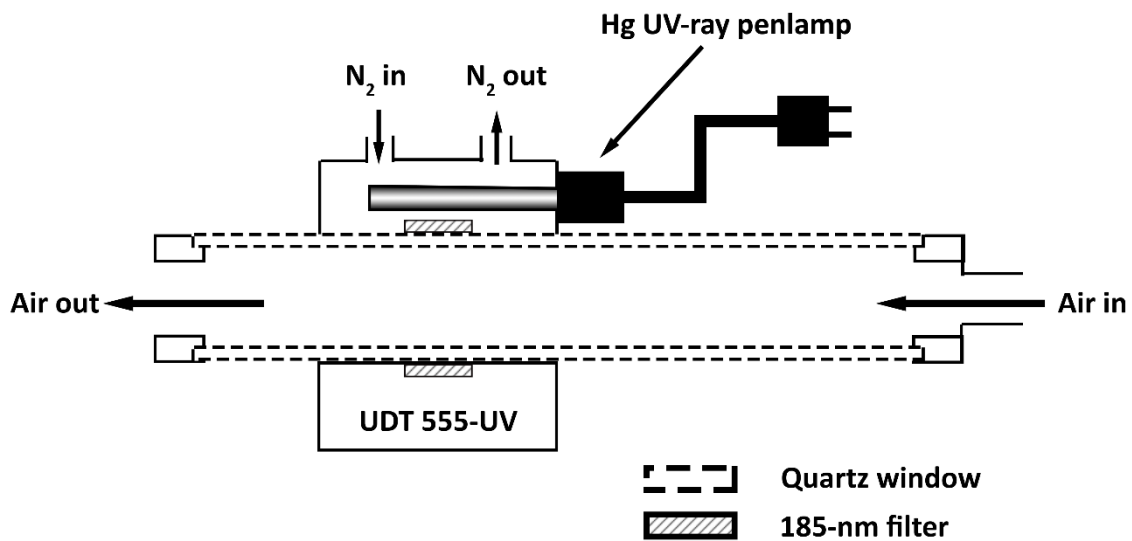
Figure 2. Cross-section of Indiana University calibration source for the IU-FAGE instrument
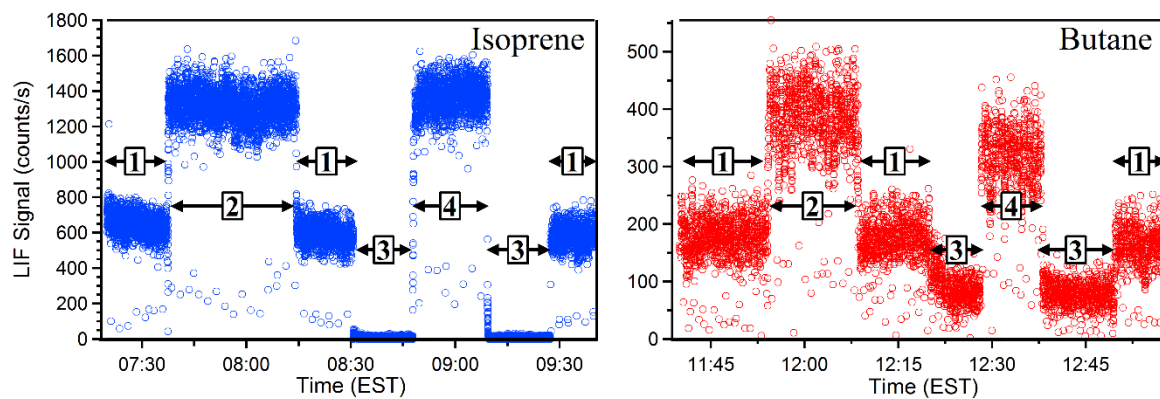
Figure 3. RO$_2$ interference measurement experiment for isoprene (left—with an OH reactivity of approximately 290 s^{-1}) and butane (right—with an OH reactivity of approximately 30 s^{-1}). The boxed numbers within the figure represents the various experimental modes: (1) S$_{OH}$, (2) S$_{HOx}$ with internal NO addition, (3) S$_{OH + VOC}$ with VOC added, (4) S$_{ROx}$ with VOC added and internal NO addition.
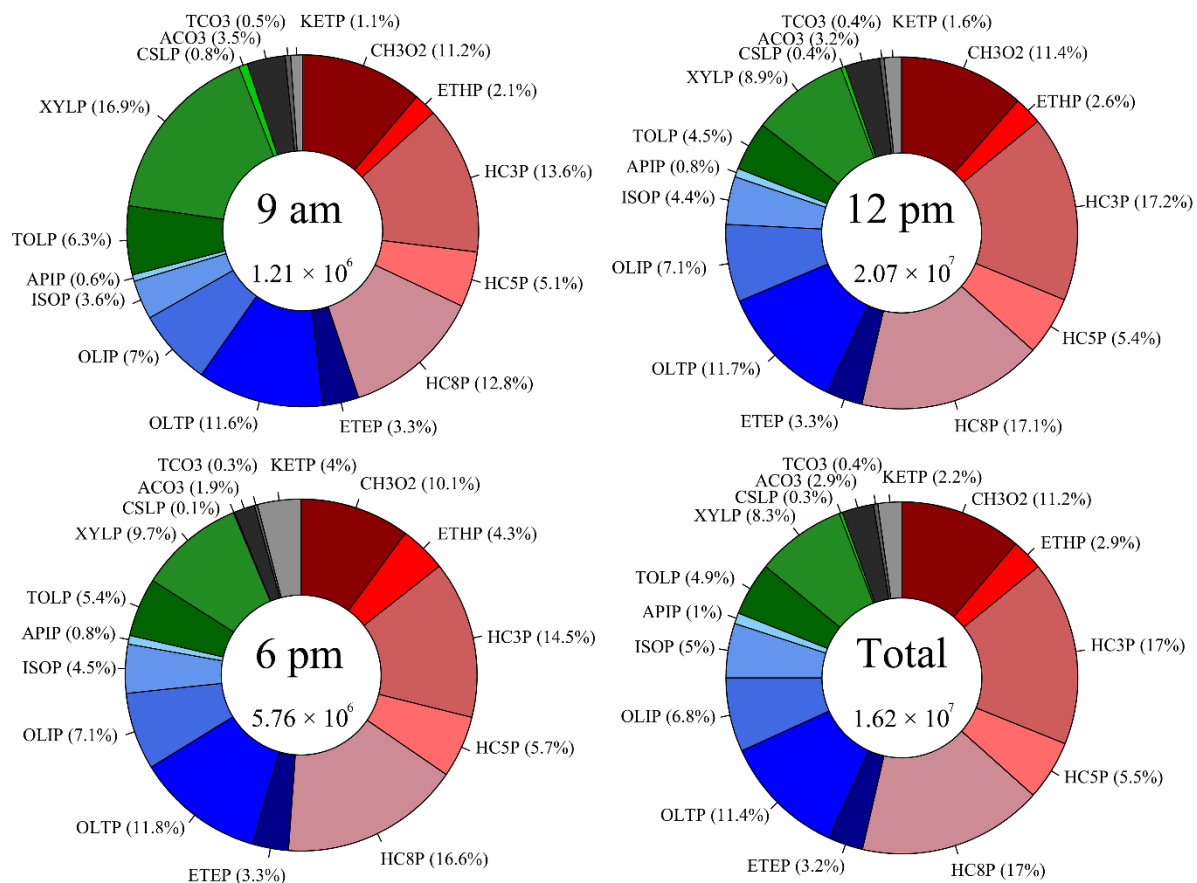
Figure 4. Modeled average peroxy radical contributions for the MCMA 2006 field campaign at 9:00 am (top left), 12:00 pm (top right), 6:00 pm (bottom left), and for the average campaign (bottom right). Shades of red represent alkanes, shades of blue represent alkenes, shades of green represent aromatics, and shades of grey represent acyl peroxy radicals. Individual RACM peroxy radical categories are defined in Section 4.2.
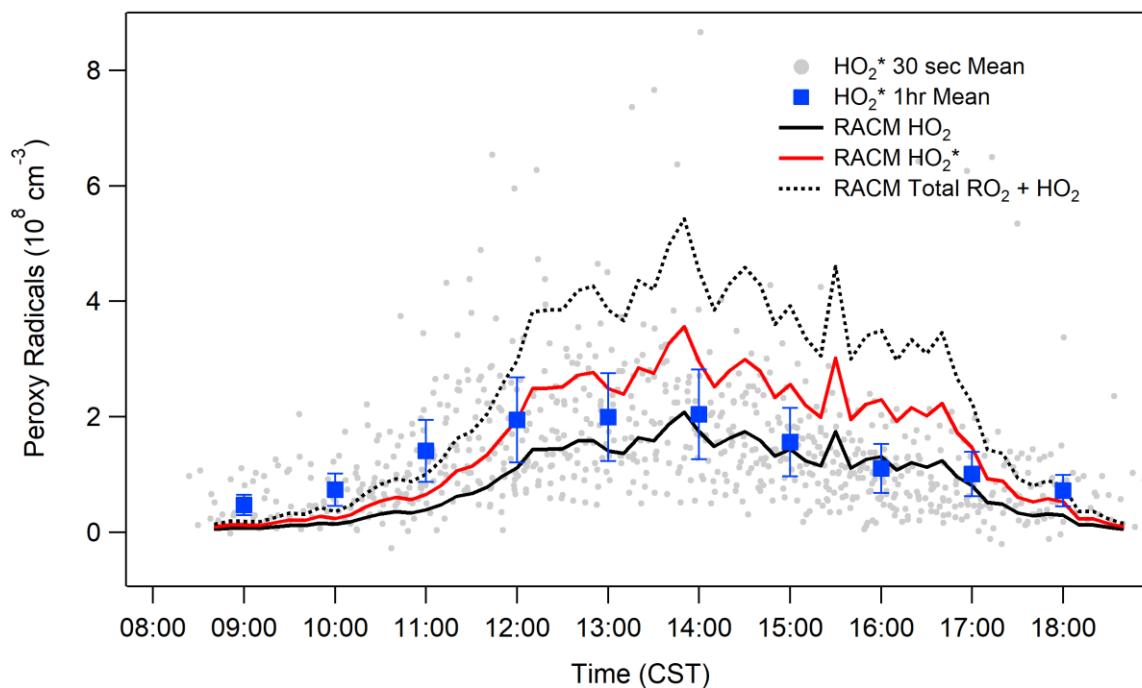
Figure 5. Diurnal average HO₂* measurements from MCMA 2006. The grey solid circles are 30 sec averages and solid blue square symbols are binned 1 hour averages. The solid black line represents the RACM modeled HO_2, the solid red line represents the modeled HO₂*, and the dotted black line represents the total modeled $RO_2 + HO_2$. The error bars reflect the calibration accuracy of the measurements ($\pm$ 36 %, 2σ).
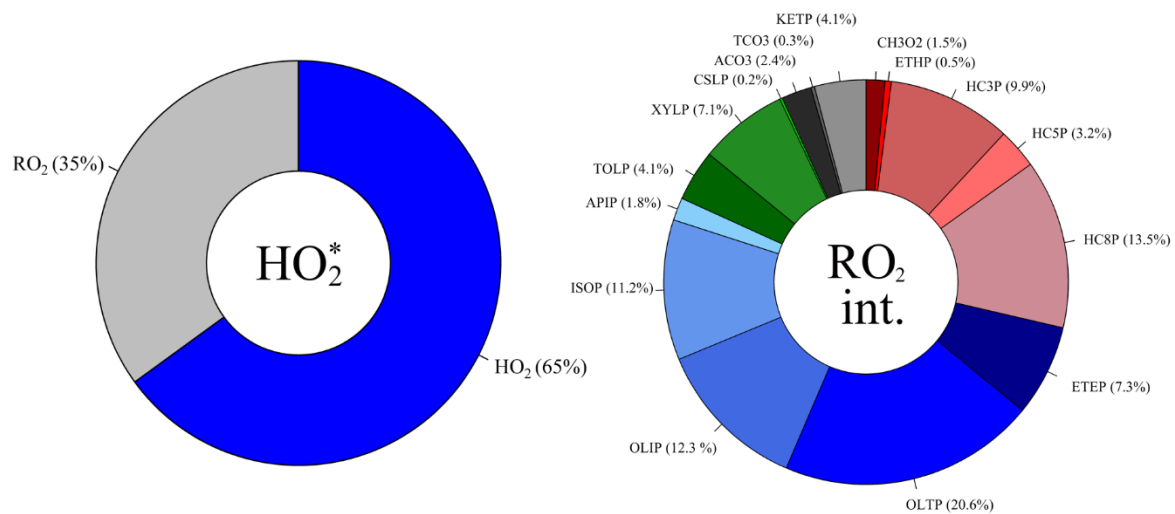
Figure 6. Modeled speciation of the RO_2 interference for MCMA 2006. The pie chart on the left is the modeled HO_2* composition after adding the fraction of RO_2 interference to the modeled HO_2. The pie chart on the right is the composition of the RO_2 interference.
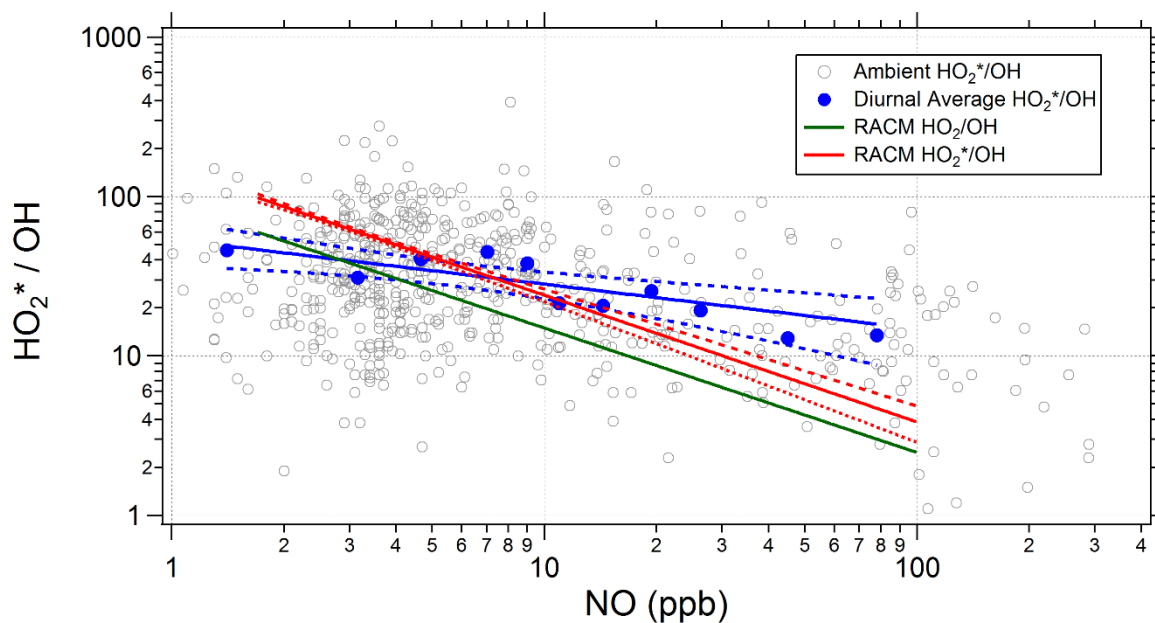
Figure 7. Correlation plot for HO$_2$*/OH vs. NO. Small grey circles are individual measurements recorded for the whole campaign. Large blue circles are average values calculated on binned NO data and the blue line is a fit to the average measurements. The model-calculated HO$_2$/OH ratio is displayed by the green line for the campaign averaged measurements, while the red line represents the modeled HO$_2$*/OH ratio. Dashed lines are the 95% confidence interval from the non-linear power regressions.